The Role of Degenerate Biradicals in the Photorearrangement of Acylcyclopropenes to Furans

Sarah Wilsey,[†] Michael J. Bearpark,[†] Fernando Bernardi,[‡] Massimo Olivucci,*[,‡] and Michael A. Robb*[,†]

Contribution from the Department of Chemistry, King's College London, Strand, London WC2R 2LS, and Dipartimento di Chimica "G. Ciamician" dell'Universita di Bologna, Via Selmi 2, 40126 Bologna, Italy

Received November 6, 1995[⊗]

Abstract: The prototype rearrangement of acylcyclopropene to furan has been studied using CAS-SCF calculations in a 6-31G* basis set. The topology and reaction funnels of the singlet ($^1(n\pi^*)$ and S_0) and triplet ($^3(n\pi^*)$ and $^3(\pi\pi^*)$) potential energy surfaces have been characterized along four possible reaction coordinates, corresponding to mechanisms where the initial step involves (a) C−O bond formation to yield an oxahousane biradical intermediate, (b) C−C bond fission to yield a 1,5 biradical intermediate, (c) C−C bond formation to yield a bicyclic intermediate, and (d) synchronous C−O and C−C bond formation to give a tricyclic intermediate. The three biradical intermediates are shallow minima on both ground and excited state surfaces. However, the most surprising result is that the reaction funnels (S_1/S_0 and T_1/S_0 crossings) are located at very similar geometries to the biradical intermediates and form the common point where decay to the ground state is possible, and where the subsequent reaction path is essentially barrierless.

Introduction

In recent experimental work, Zimmerman and co-workers,[1,2] have investigated the mechanism of the photochemical rearrangement of acylcyclopropenes[3] to furans by examining substituent effects. From a theoretical point of view, the understanding of such isomerizations is of fundamental importance because acylcyclopropenes have two different chromophores (alkene and carbonyl) that can be excited. Accordingly, three different excited state surfaces must be involved: the singlet and triplet $n\pi^*$ surfaces where the excitation is centered on the carbonyl moiety, and the triplet $\pi\pi^*$ surface where the excitation is centered on the alkene moiety. While experimental work[1,2] can suggest a sequence of structures that occur along the reaction path, it cannot establish whether these structures are intermediates or transition states, or whether they lie on the excited state branch of the reaction path or the ground state. Our objective in this work is to establish the topology and energetics of the singlet and triplet potential energy surfaces along four possible reaction coordinates (A−D in Scheme 1) for a "model" acylcyclopropene with no substituent groups. For each mechanism, we have also located the regions on the potential surface where the molecule can decay from the excited state to the ground state surface, via singlet/singlet crossings (conical intersections[4−7]) or singlet/triplet crossings.

Zimmerman et al.[1,2] have shown that thioxanthone sensitization of acylcyclopropenes produces furans, provided there is an aryl substituent at C_3 (Scheme 2). Prior to their work only dimerization of acylcyclopropenes had been observed on triplet sensitization,[8] although furans had been observed on direct photolysis. They found that sensitization[1,2] of 3-acetyl-1,2-diphenyl-3-*p*-tolylcyclopropene (**1**) and 3-acetyl-2,3-diphenyl-1-*p*-tolylcyclopropene (**2**) gave exclusively 2,3-diphenyl-4-tolylfuran (**3**) in the first case and a mixture of 3,4-diphenyl-

Scheme 1

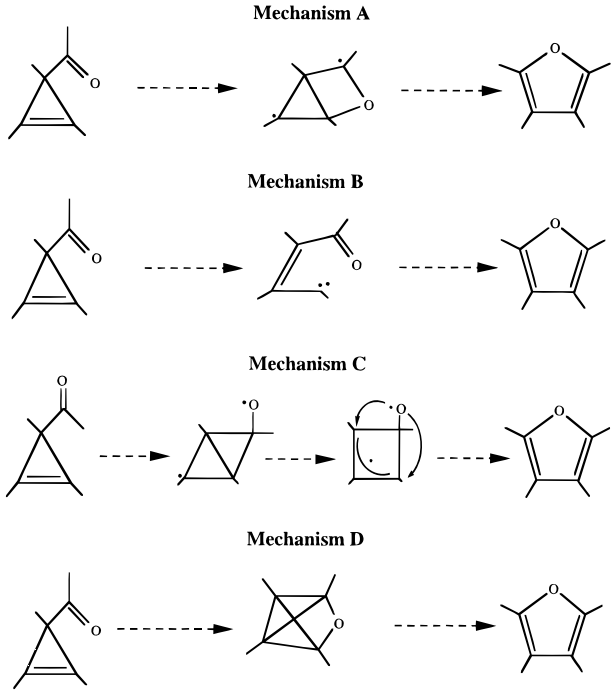

[†] King's College London.
[‡] Universita di Bologna.
[⊗] Abstract published in *Advance ACS Abstracts,* April 1, 1996.

(1) Zimmerman, H. E.; Wright, C. W. *J. Am. Chem. Soc.* **1992**, *114*, 363−365.
(2) Zimmerman, H. E.; Wright, C. W. *J. Am. Chem. Soc.* **1992**, *114*, 6604.
(3) The photochemistry of acylcyclopropenes is of interest since these molecules are thought to be intermediates in the photochemical isomerizations of five-membered rings—see for example: Rendall, W. A.; Torres, M.; Lown, E. M.; Struasz, O. P. *Rev. Chem. Intermed.* **1986**, *6*, 335−364.
(4) Zimmerman, H. E. *J. Am. Chem. Soc.* **1966**, *88*, 1566.
(5) Michl, J. *J. Mol. Photochem.* **1972**, 243.
(6) Teller, E. *Isr. J. Chem.* **1969**, *7*, 227.
(7) (a) Von Neumann, J.; Wigner, E. *Phys. Z.* **1929**, *30*, 467; (b) Teller, E. *J. Phys. Chem.* **1937**, *41*, 109; (c) Herzberg, G.; Longuet-Higgins, H. C. *Trans. Faraday Soc.* **1963**, *35*, 77; (d) Atchity, G. J.; Xantheas, S. S.; Ruedenberg, K. *J. Chem. Phys.* **1991**, *95*, 1862.
(8) DeBoer, C. D.; Wadsworth, D. H.; Perkins, W. C. *J. Am. Chem. Soc.* **1973**, *95*, 861.

S0002-7863(95)03726-7 CCC: $12.00

Scheme 2

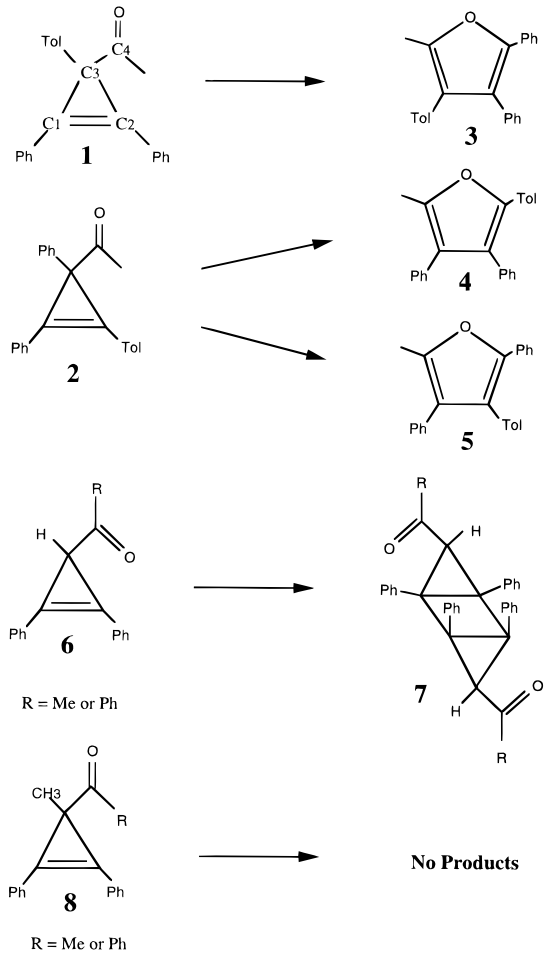

2-tolylfuran (**4**) and 2,4-diphenyl-3-tolylfuran (**5**) in the second. In cases where C_3 was unsubstituted (**6** in Scheme 2), thioxanthone sensitization gave only triplet dimerization products (**7**). The lack of dimerization products observed in cases where C_3 is substituted was thought to be the result of steric effects. On the other hand, methyl substitution at C_3 (**8**) rendered the molecule completely unreactive on thioxanthone sensitization.

Four different mechanisms (A−D in Scheme 1) for the rearrangement to furans have been postulated by Zimmerman. An oxadi-π-methane type mechanism, involving initial carbon−carbon bond formation (Mechanism C) has been established for the analogous rearrangement of triplet vinylcyclopropenes.[9] However, the products formed on triplet sensitization of acylcyclopropenes appear to result from a mechanism involving initial oxygen attack proceeding through an oxahousane biradical intermediate (Mechanism A). The absence of photoproducts observed when C_3 is methylated can then be explained in terms of the two possible conformers that can exist, i.e. the oxygen can be either syn or anti to the three-membered ring. In order to produce the oxahousane intermediate the oxygen would need to be syn to the ring, but in the case of 3-methyl-substituted acylcyclopropenes, the favored conformer appears to be the anti.

In contrast, the singlet reaction gives a variety of side products.[10] It is thought to take place via a mechanism that involves initial bond fission in the three-membered ring to form a carbene biradical, followed by subsequent formation of the C−O bond (Mechanism B). This mechanism also predicts the correct photoproducts for the triplet reaction, since it only differs from Mechanism A by the order in which the C−C bond is broken and the C−O bond is formed. However, it was excluded for the case of the triplet, as previous studies[11] had shown that triplet cyclopropenes do not undergo ring fission and no side products were observed. The remaining possibility is Mechanism D, a synchronous Paterno−Buchi type rearrangement[12] involving a tricyclic intermediate. This was also excluded by Zimmerman as not all of the products predicted by this mechanism were observed on photolysis.

Scheme 3

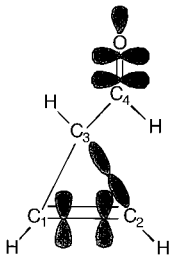

Computational Details

The potential energy surface of the model acylcyclopropene was investigated using the MC-SCF code implemented in Gaussian94,[13] with a complete active space (CAS) configuration interaction expansion using eight electrons in seven orbitals and a 6-31G* basis set. The active orbitals chosen were the four π orbitals, an n orbital on the oxygen atom, and the σ orbitals in the C_3-C_2 bond as illustrated in Scheme 3. At some structures (labeled with footnote *a* in Table 1), one of the orbitals was doubly occupied and so the geometries were optimized in a smaller active space of six orbitals and six electrons. Single points were then run in the full active space to give a comparable energy. As all the substituent groups were taken to be hydrogen, breaking the C_3-C_2 bond was assumed to be exactly equivalent to breaking the C_1-C_3 bond, and therefore we only studied that part of the potential surface corresponding to C_2-C_3 bond cleavage.

Our study involved the location of minima, transition structures, conical intersections (singlet/singlet crossing points), and singlet/triplet crossing points. The minima and transition states were characterized by frequency calculations, and intrinsic reaction coordinate (IRC) calculations were run from each transition structure.

The funnel that controls the radiationless decay process from an upper to a lower electronic state corresponds to a conical intersection or a singlet/triplet crossing point. The method used to optimize the lowest energy point of such crossings has been discussed elsewhere[14] (see ref 15 for recent examples). The crossing of two states of the same spin multiplicity is characterized by the gradient difference vector and the non-adiabatic coupling matrix element which are obtained as part of the optimization process. Distortion of the molecular geometry along these directions lifts the degeneracy, and the initial relaxation path after decay through a crossing will lie in this space. The same method was used to characterize the singlet/triplet crossings, although the non-adiabatic coupling at these points is zero. The spin−orbit coupling

(9) Zimmerman, H. E.; Fleming, S. A. *J. Am. Chem. Soc.* **1983**, *105*, 363.

(10) Padwa, A.; Akiba, M.; Chou, C. S.; Cohen, L. *J. Org. Chem.* **1982**, *47*, 183- 191.

(11) Pincock, J. A.; Boyd, R. J. *Can. J. Chem.* **1977**, *55*, 2482−2491.

(12) (a) Paterno, E.; Chieffi, G. *Gazz. Chim. Ital.* **1909**, *39*, 341. (b) Buchi, G.; Inman, C. G.; Lipinsky, E. S. *J. Am. Chem. Soc.* **1954**, *76*, 4327−4331.

(13) *Gaussian94*, Revision B; Frisch, M. J.; Trucks, G. W.; Schlegel, H. B.; Gill, P. M. W.; Johnson, B. G.; Robb, M. A.; Cheeseman, J. R.; Keith, T.; Petersson, G. A.; Montgomer, J. A.; Raghavachari, K.; Al-Laham, M. A.; Zakrzewski, V. G.; Ortiz, J. V.; Foresman, J. B.; Cioslowski, A.; Stefanov, B. B.; Nanayakkara, A.; Challacombe, M.; Peng, C. Y.; Ayala, P. Y.; Chen, W.; Wong, M. W.; Andres, J. L.; Replogle, E. S.; Gomperts, R.; Martin, R. L.; Fox, D. J.; Binkley, J. S.; Defrees, D. J.; Baker, J.; Stewart, J. J.; Head-Gordon, M.; Gonzalez, C.; Pople, J. A.; Gaussian, Inc.: Pittsburgh, PA, 1995.

(14) (a) Ragazos, I. N.; Robb, M. A.; Bernardi, F.; Olivucci, M. *Chem. Phys. Lett.* **1992**, *197*, 217. (b) Yarkony, R. D. *J. Phys. Chem.* **1993**, *97*, 4407. (c) Bearpark, M. J.; Robb, M. A.; Schlegel, H. B. *Chem. Phys. Lett.* **1994**, *223*, 269.

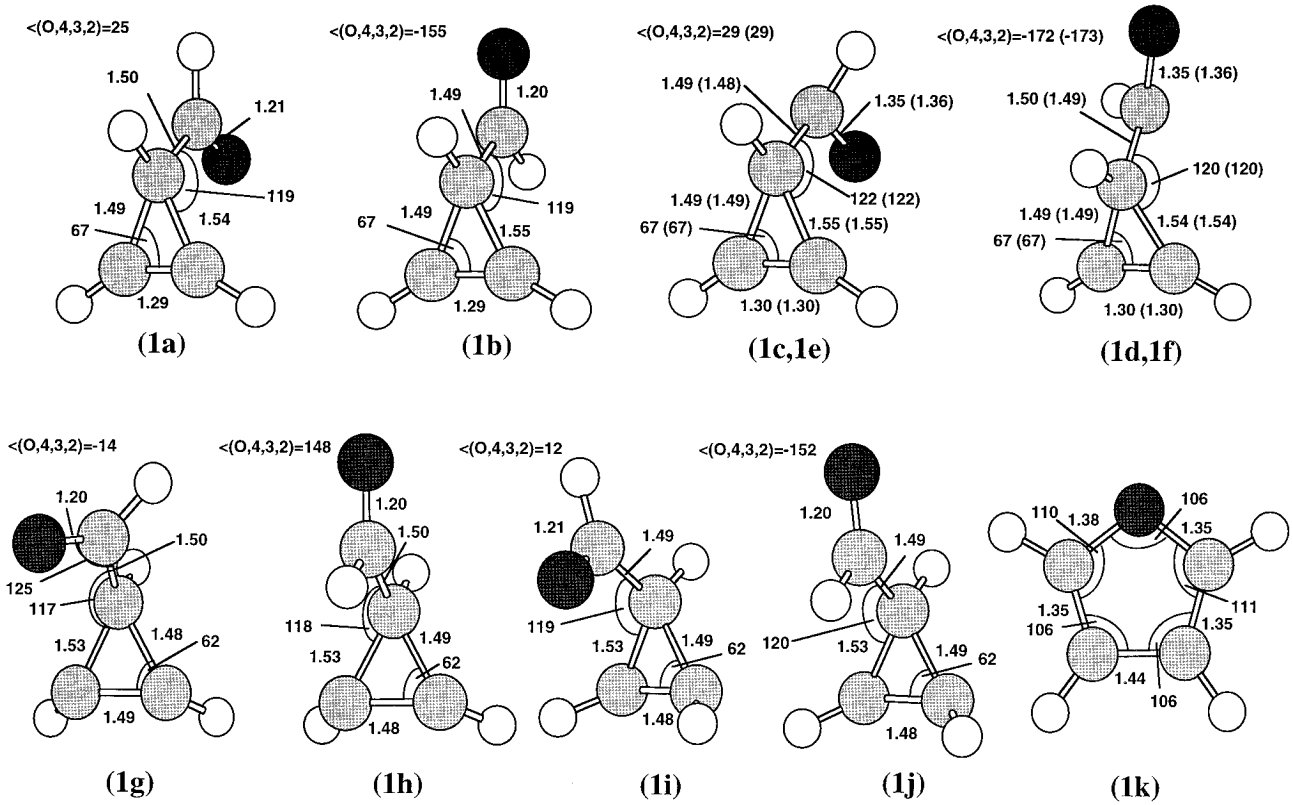

Figure 1. Optimized structures of reactant minima and products (bond lengths in angstroms and angles in degrees): (a) S_0 reactant molecule in syn conformation; (b) S_0 reactant molecule in anti conformation; (c) $^3(n\pi^*)$ reactant minimum with syn conformation; (d) $^3(n\pi^*)$ reactant minimum with anti conformation; (e) $^1(n\pi^*)$ reactant minimum with syn conformation; (f) $^1(n\pi^*)$ reactant minimum with anti conformation; (g) $^3(\pi\pi^*)$ reactant minimum with syn conformation (trans); (h) $^3(\pi\pi^*)$ reactant minimum with anti conformation (trans); (i) $^3(\pi\pi^*)$ reactant minimum with syn conformation (cis); (j) $^3(\pi\pi^*)$ reactant minimum with anti conformation (cis); (k) furan (product). (At similar structures, singlet geometries are given in parentheses after the triplet geometries.)

constant was calculated at the singlet/triplet crossing points using a one-electron approximation with the effective nuclear charges O: 5.6 and C: 3.6, as optimized by Koseki et al.[16] Yarkony[17] has shown, using a Landau−Zener formalism, that the efficiency of intersystem crossing is proportional to the magnitude of the spin−orbit coupling, and is most favorable when the gradient difference is small and the kinetic energy of the nuclei is low. Typical favorable spin−orbit coupling between singlet and triplet states with the same electronic configuration will be ca. $1-2$ cm^{-1} corresponding to a lifetime of 30 ps. However, as we shall discuss subsequently, if the electronic configurations are different the spin−orbit coupling will be much larger. Thus the other factors in the Landau−Zener formula (kinetic energy and gradient difference) may play an important role in the efficiency of intersystem crossing.

Results and Discussion

Minima, transition states, and surface crossings for the four mechanisms (A−D) have been located for the $^3(n\pi^*)$, $^3(\pi\pi^*)$, and $^1(n\pi^*)$ states of acylcyclopropene. The energies are given in Table 1 and the corresponding optimized structures are illustrated in Figures 1−5.

The geometries at the reactant minima on the ground and excited state surfaces (Figure 1a−j) can have the oxygen atom syn (Figure 1a,c,e,g,i) or anti (Figure 1b,d,f,h,j) to the three-membered ring. Mechanisms A and B would occur from the syn conformers as they involve attack of the oxygen atom at C_2, whereas Mechanism C could occur from either the syn or the anti conformers leading to an endo or exo mechanism, respectively. There are two additional isomers that need to be considered on the $\pi\pi^*$ surface, since the hydrogen atoms at the C_1C_2 bond can either be trans (Figure 1g,h) or cis (Figure 1i,j) to the carbonyl group. However, the energy difference between all the different isomers is less than 3 kcal mol^{-1} in each case, and in real systems the most favored conformer will depend on the substituent groups present. The reference energies given in Table 1 correspond to the energies on T_1, S_1, and T_2 calculated at the syn structure of the reactant molecule on the ground state surface (Figure 1a).

Mechanism A: The Oxahousane Pathway. Zimmerman et al.[1,2] suggest that the rearrangement of acylcyclopropene to furan on triplet sensitization should occur via a pathway

(15) (a) Bernardi, F.; De, S.; Olivucci, M.; Robb, M. A. *J. Am. Chem. Soc.* **1990**, *112*, 1737. (b) Reguero, M.; Bernardi, F.; Bottoni, A.; Olivucci, M.; Robb, M. A. *J. Amer. Chem. Soc.* **1991**, *113*, 1566 (c) Bernardi, F.; Ragazos, I. N.; Olivucci, M.; Robb, M. A. *J. Am. Chem. Soc.* **1992**, *114*, 2752. (d) Bernardi, F.; Olivucci, M.; Robb, M. A. *J. Am. Chem. Soc.* **1992**, *114*, 5805. (e) Bernardi, F.; Olivucci, M.; Palmer, I. J.; Robb, M. A. *J. Org. Chem.* **1992**, *57*, 5081. (f) Bernardi, F.; Ragazos, I. N.; Olivucci, M.; Robb, M. A. *J. Am. Chem. Soc.* **1992**, *114*, 8211. (g) Palmer, I. J.; Ragazos, I. N.; Bernardi, F.; Olivucci, M.; Robb, M. A. *J. Am. Chem. Soc.* **1993**, *115*, 673. (h) Reguero, M.; Bernardi, F.; Jones, H.; Olivucci, M.; Robb, M. A. *J. Am. Chem. Soc.* **1993**, *115*, 2073. (i) Olivucci, M.; Ragazos, I. N.; Bernardi, F.; Robb, M. A. *J. Am. Chem. Soc.* **1993**, *115*, 3710 (j) Bernardi, F.; Olivucci, M.; Robb, M. A. *Isr. J. Chem.* **1993**, *33*, 256. (k) Olivucci, M.; Bernardi, F.; Ragazos, I. N.; Robb, M. A. *J. Am. Chem. Soc.* **1994**, *116* 1077. (l) Bernardi, F.; Bottoni, A.; Olivucci, M.; Venturini, A.; Robb, M. A. *J. Chem. Soc., Faraday Trans.* **1994**, *90*, 1617. (m) Palmer, I. J.; Bernardi, F.; Olivucci, M.; Ragazos, I. N.; Robb, M. A. *J. Am. Chem. Soc.* **1994**, *116*, 2121. (n) Olivucci, M.; Bernardi, F.; Ottani, S.; Robb, M. A. *J. Am. Chem. Soc.* **1994**, *116*, 2034. (o) Yamamoto, N.; Bernardi, F.; Olivucci, M.; Robb, M. A.; Wilsey, S. *J. Am. Chem. Soc.* **1994**, *116*, 2064. (p) Reguero, M.; Olivucci, M.; Bernardi, F.; Robb, M. A. *J. Am. Chem. Soc.* **1994**, *116*, 2103. (q) Celani, P.; Ottani, S.; Olivucci, M.; Bernardi, F.; Robb, M. A. *J. Am. Chem. Soc.* **1994**, *116*, 10141. (r) Bearpark, M. J.; Olivucci, M.; Wilsey, S.; Bernardi, F.; Robb, M. A.; *J. Am. Chem. Soc.* **1995**, *117*, 6944. (s) Wilsey, S.; Bearpark, M. J.; Bernardi, F.; Olivucci, M.; Robb, M. A. *J. Am. Chem. Soc.* **1996**, *118*, 176.

(16) Koseki, S.; Schmidt, M. W.; Gordon, M. S. *J. Phys. Chem.* **1992**, *96*, 10768.

(17) Yarkony, D. R. *J. Am. Chem. Soc.* **1992**, *114*, 5406.

Table 1. Energetics for Reactions from the $^3(n\pi^*)$, $^1(n\pi^*)$, and $^3(\pi\pi^*)$ Surface

geometry	surface	energy (hartrees)	energy (kcal mol^{-1})
(a) $^3(n\pi^*)$ Surface			
			rel to $^3(n\pi^*)$ vertical excitation
syn equilibrium geometry	S_0	−228.6345	−94.3
of reactant molecule (Figure 1a)	$^3(n\pi^*)$	−228.4843	**0.0**
anti equilibrium geometry	S_0	−228.6365	−95.5
of reactant molecule (Figure 1b)	$^3(n\pi^*)$	−228.4839	+0.3
syn minimum (Figure 1c)	$^3(n\pi^*)$	−228.5123	−17.6
anti minimum (Figure 1d)	$^3(n\pi^*)$	−228.5108	−16.6
furan (Figure 1k)	S_0	−228.7104	−141.9
Mechanism A			
transition state (Figure 2a)	$^3(n\pi^*)$	−228.4691	+9.5
S_0/T_1 crossing point (Figure 2d)	$^3(n\pi^*)$	−228.4956	−7.1
	S_0	−228.4958	−7.2
intermediate (Figure 2e)	$^3(n\pi^*)$	−228.4974	−8.2
intermediate (Figure 2f)	S_0	−228.5066	−14.0
transition state to furan (Figure 2g)	$^3(n\pi^*)$	−228.4883	−2.5
(Figure 2h)	S_0	−228.4883	−2.5
Mechanism B			
transition state (Figure 3a)	$^3(n\pi^*)$	−228.5002	−10.0
minimum (Figure 3c)	$^3(n\pi^*)$	−228.5486	−40.3
S_1/T_2 crossing (Figure 3e)	$^1(n\pi^*)$	−228.5486	−40.3
	$^3(n\pi^*)$	−228.5486	−40.3
Mechanism C (endo pathway)			
transition state (Figure 4b)	$^3(n\pi^*)$	−228.4626[a]	+13.6
T_2/T_1 crossing point (Figure 4e)	$^3(n\pi^*)$	−228.4972	−8.1
	$^3(\pi\pi^*)$	−228.4973	−8.2
minimum (Figure 4g)	$^3(n\pi^*)$	−228.5010	−10.5
minimum (Figure 4h)	S_0	−228.5046	−12.7
transition state (Figure 4j)	S_0	−228.4932	−5.6
minimum (Figure 4l)	S_0	−228.5905[a]	−66.6
transition state (Figure 4m)	S_0	−228.5528[a]	−43.0
Mechanism D			
tricyclic intermediate (Figure 5a)	S_0	−228.5436	−37.2
(b) $^1(n\pi^*)$ Surface			
			rel to $^1(n\pi^*)$ vertical excitation
syn equilibrium geometry	S_0	−228.6345	−100.9
of reactant molecule (Figure 1a)	$^1(n\pi^*)$	−228.4737	**0.0**
anti equilibrium geometry	S_0	−228.6365	−102.2
of reactant (Figure 1b)	$^1(n\pi^*)$	−228.4727	+0.6
syn minimum (Figure 1e)	$^1(n\pi^*)$	−228.5042	−19.1
anti minimum (Figure 1f)	$^1(n\pi^*)$	−228.5019	−17.7
furan (Figure 1k)	S_0	−228.7104	−148.5
Mechanism A			
transition state (Figure 2b)	$^1(n\pi^*)$	−228.4568[b]	+10.6
S_1/S_0 crossing (Figure 2c)	$^1(n\pi^*)$	−228.4633	+6.5
	S_0	−228.4636	+6.3
intermediate (Figure 2f)	S_0	−228.5066	−20.6
(Figure 2h)	S_0	−228.4883	−9.2
Mechanism B			
transition state (Figure 3b)	$^1(n\pi^*)$	−228.4942[b]	−12.9
minimum (Figure 3d)	$^1(n\pi^*)$	−228.5507	−48.3
S_1/T_2 crossing (Figure 3e)	$^1(n\pi^*)$	−228.5486	−47.0
	$^3(n\pi^*)$	−228.5486	−47.0
conical intersection (Figure 3f)	$^1(n\pi^*)$	−228.5668	−58.4
	S_0	−228.5668	−58.4
minimum (Figure 3g)	S_0	−228.5829	−68.5
Mechanism C (endo pathway)			
transition state (Figure 4c)	$^1(n\pi^*)$	−228.4550[b]	+11.7
S_1/S_0 crossing point (Figure 4d)	$^1(n\pi^*)$	−228.4963	−14.2
	S_0	−228.4965	−14.3
minimum (Figure 4h)	S_0	−228.5046	−19.4
transition state (Figure 4j)	S_0	−228.4932	−12.2
minimum (Figure 4l)	S_0	−228.5905[a]	−73.2
transition state (Figure 4m)	S_0	−228.5528[a]	−49.6

Table 1 (Continued)

geometry	surface	energy (hartrees)	energy (kcal mol^{-1})
	(c) ^{3}(nπ*) Surface		
			rel to $^3(\pi\pi^*)$ vertical excitation
syn equilibrium geometry	S_0	−228.6345	−105.8
of reactant (Figure 1a)	$^3(\pi\pi^*)$	−228.4659	**0.0**
anti equilibrium geometry	S_0	−228.6365	−107.1
of reactant (Figure 1b)	$^3(\pi\pi^*)$	−228.4692	−2.1
syn minimum (trans) (Figure 1g)	$^3(\pi\pi^*)$	−228.5276	−38.7
anti minimum (trans) (Figure 1h)	$^3(\pi\pi^*)$	−228.5320	−41.5
syn minimum (cis) (Figure 1i)	$^3(\pi\pi^*)$	−228.5324	−41.7
anti minimum (cis) (Figure 1j)	$^3(\pi\pi^*)$	−228.5323	−41.7
furan (Figure 1k)	S_0	−228.7104	−153.4
Mechanism B			
transition state (Figure 3h)	$^3(\pi\pi^*)$	−228.5042	−24.0
minimum (Figure 3i)	$^3(\pi\pi^*)$	−228.5843	−74.2
minimum (Figure 3j)	S_0	−228.5816	−72.6
T_1/S_0 crossing (Figure 3k)	$^3(\pi\pi^*)$	−228.5817	−72.7
	S_0	−228.5814	−72.4
minimum (Figure 3l)	$^3(\pi\pi^*)$	−228.6059	−87.9
minimum (Figure 3g)	S_0	−228.5829	−73.4
Mechanism C (endo pathway)			
transition state (Figure 4a)	$^3(\pi\pi^*)$	−228.4922	−16.5
minimum (Figure 4f)	$^3(\pi\pi^*)$	−228.5058	−25.0
minimum (Figure 4h)	S_0	−228.5046	−24.3
transition state (Figure 4i)	$^3(\pi\pi^*)$	−228.4897	−14.9
transition state (Figure 4j)	S_0	−228.4932	−17.1
square intermediate (Figure 4k)	$^3(\pi\pi^*)$	−228.5556	−56.3
	S_0	−228.5559	−56.5
minimum (Figure 4l)	S_0	−228.5905[a]	−78.2
transition state (Figure 4m)	S_0	−228.5528[a]	−54.5

[a] Structures optimized in (6,6) active space and single points run in (8,7) active space. [b] Structures optimized using state-averaged orbitals and single points run without.

involving initial C−O bond formation leading to an oxahousane biradical intermediate. A sketch of the reaction coordinate from the ^{3}(nπ*) and ^{1}(nπ*) surfaces can be found in Figure 6.

The results in Table 1 show that, on the ^{3}(nπ*) surface, the oxahousane biradical intermediate (Figure 2e) is accessible over a 27 kcal mol^{-1} barrier from the ^{3}(nπ*) acylcyclopropene syn minimum (Figure 1c). The $^3(\pi\pi^*)$ surface appears to becompletely repulsive along this coordinate and we were unable to locate a transition state leading to the corresponding triplet oxahousane intermediate on this surface.

The oxahousane structure (Figure 2d,e,f) forms the focal point of Mechanism A. Remarkably, this structure is a quasidegenerate biradical. There is both a ^{3}(nπ*)/S_0 crossing point (Figure 2d) and an intermediate on both the ^{3}(nπ*) state (Figure 2e) and ground state (Figure 2f) surfaces with similar geometries. The spin−orbit coupling constant computed at the crossing point is 2 cm^{-1}, which is relatively large considering the structures are just two different states of a biradical. Therefore ISC is expected to be reasonably efficient at this point. Transition states leading from the oxahousane intermediate to furan were located on T_1(nπ*) (Figure 2g) and S_0 (Figure 2h) at energies of 6 and 11 kcal mol^{-1} above the intermediate structures, respectively. These barriers corresponded to cleavage of the C_3-C_2 bond and planarization, leading to triplet or ground state furan.

Although the rearrangement on direct photolysis is assumed to involve initial bond fission of the three-membered ring (Mechanism B), our results demonstrate that the reaction coordinate corresponding to Mechanism A can also be populated on the ^{1}(nπ*) surface. The ^{1}(nπ*) excited state minimum (Figure 1e) and the transition state (Figure 2b) leading to the oxahousane structure were located at very similar geometries as the analogous structures on the ^{3}(nπ*) surface (Figure 1c,a). However, the reaction path from the transition state (Figure 2b) leading toward the oxahousane biradical on S_0 (Figure 2e) passes through a ^{1}(nπ*)/S_0 conical intersection structure (Figure 2c) when the O−C_2 distance is about 1.65 Å. At this point fully efficient internal conversion is possible and the gradient difference and non-adiabatic coupling vectors (Figure 2c) indicate that the degeneracy is lifted by O−C_2 motion leading to either the reactant molecule (Figure 1a) or the oxahousane minimum (Figure 2f) forming furan.

Mechanism B: Initial Ring-Fission Pathway. Mechanism B corresponds to initial C_2-C_3 σ bond fission. For vinylcyclopropenes it is known to be the reaction coordinate on direct photolysis, and Zimmerman et al.[1,2] suggest the involvement of a carbene intermediate following the initial excitation of the S_1 ($\pi\pi^*$ ionic/Rydberg) state. However, in acylcyclopropenes, this type of singlet mechanism is unlikely to occur because the initial state populated on direct photolysis will be the ^{1}(nπ*) state. We will show that fission pathways exist on both the ^{1}(nπ*) and ^{3}(nπ*) surfaces, as well as on the $^3(\pi\pi^*)$ surface (see Figure 7). The triplet mechanisms involve twisted 1,5-biradicaloid intermediates where there are triplet/singlet crossing points (^{3}(nπ*)/^{1}(nπ*) and $^3(\pi\pi^*)/S_0$). Decay from the ^{1}(nπ*) surface to the ground state surface occurs through a conical intersection at a planar 1,5-biradicaloid structure leading to a planar intermediate on the ground state, close to the intersection geometry. For the unsubstituted acylcyclopropene, the first intermediate is biradicaloid with the unpaired electrons on different centers (O and C_2), rather than carbene-like with the unpaired electrons on the same center (C_2), as suggested by Zimmerman for the case of aryl-substituted vinylcyclopropenes.

The barriers (Figure 3a,b) on the triplet and singlet nπ* surfaces leading to the twisted intermediates (Figure 3c, 3d) lie 8 and 6 kcal mol^{-1} above the excited state minima (Figure 1c,e)

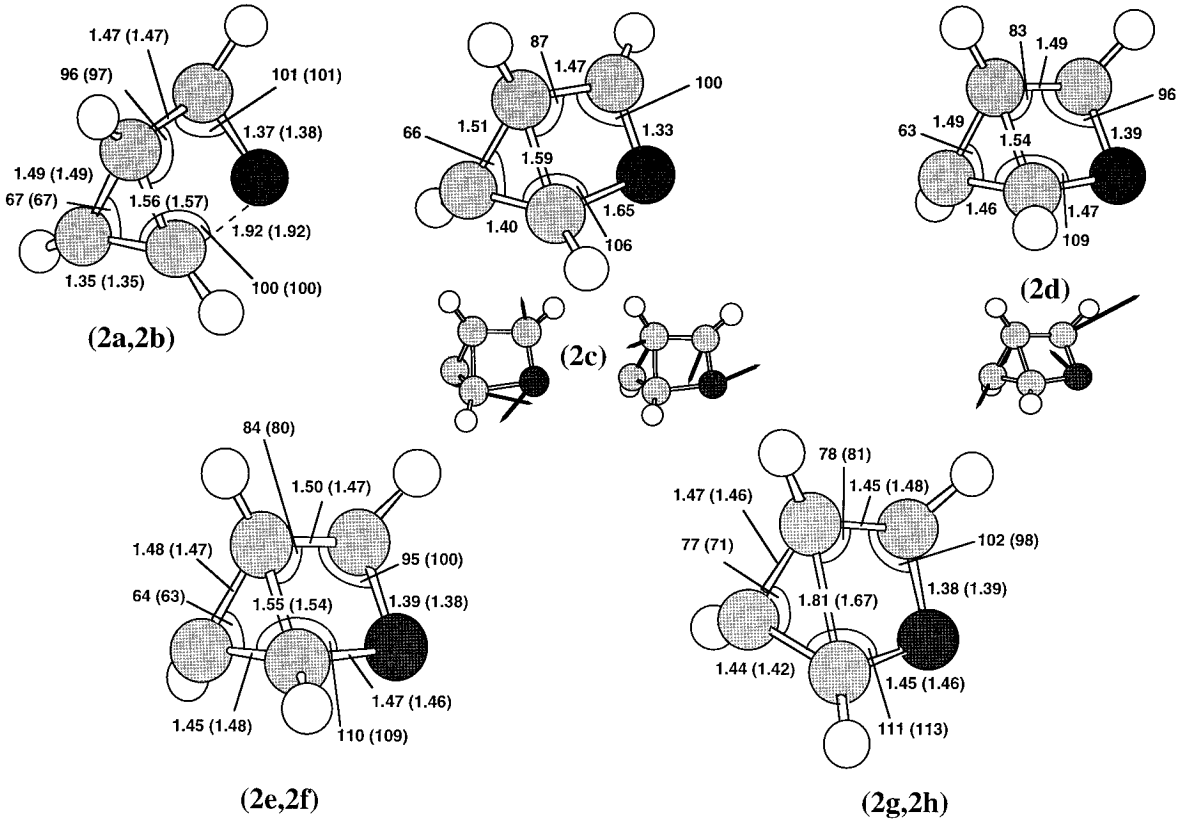

Figure 2. Optimized structures for oxahousane mechanism (bond lengths in angstroms and angles in degrees): (a) reactant minimum (syn)−oxahousane intermediate transition state on $^3(n\pi^*)$ surface; (b) reactant minimum (syn)−oxahousane intermediate transition state on $^1(n\pi^*)$ surface; (c) conical intersection close to oxahousane intermediate (with derivative coupling and gradient difference vectors shown below); (d) $^3(n\pi^*)/^1(n\pi^*)$ crossing point at oxahousane intermediate (with gradient difference vector shown below); (e) oxahousane intermediate on $^3(n\pi^*)$ surface; (f) oxahousane intermediate on S_0; (g) oxahousane intermediate−furan transition state on $^3(n\pi^*)$ surface; (h) oxahousane intermediate−furan transition state on S_0. (At similar structures, singlet geometries are given in parentheses after the triplet geometries.)

respectively, and correspond to the breaking of the C_2-C_3 bond. At these intermediate structures the carbonyl group is perpendicular to the $C_1-C_2-C_3$ plane and there is a new π bond formed between C_3 and C_4. Frequency calculations run at these points showed that the surface is very flat in this region as there is almost free rotation about the C_1-C_3 bond. At this geometry the singlet and triplet $n\pi^*$ states are degenerate with one unpaired electron on C_2 and one in the oxygen n orbital, but as they are two states of a perfect biradical the spin−orbit coupling between them is very small (<1 cm^{-1}). However, as the two surfaces are very flat and degenerate over a wide range of geometries, the probability of ISC from the triplet to the singlet surface could be relatively high.

On the $^1(n\pi^*)$ surface, the carbonyl group can then rotate about the C_1-C_3 bond with virtually no barrier to reach the planar conical intersection structure (Figure 3f). At the conical intersection the π electrons in the new C_3-C_4 π bond become delocalized over the carbonyl group. The C−O bond shortens and the C_3-C_4 bond length increases such that both the C−O π bond and the C_4-C_3 π bond are partially formed, with one unpaired electron on C_2 and the other delocalized between the oxygen atom and C_3 (i.e. this structure is more diradicaloid than carbene-like). At this point fully efficient decay to the ground state surface is possible, and the directions of the derivative coupling and gradient difference vectors (Figure 3f) indicate the plane of initial relaxation on the ground state. The ground state path involves a barrierless process leading to furan (Figure 1k) which involves completely breaking the C−O π bond, and coupling the unpaired electrons on the oxygen atom and C_2 to form the five-membered ring. Alternatively, the molecule can fall into an adjacent minimum on S_0 (Figure 3g) where the C−O π bond has reformed and the new C_4-C_3 π bond has broken, leaving the unpaired electrons on C_2 and C_3. This intermediate is separated from the reactant molecule by a small energy barrier which we could not fully optimize as it appears to be very close to the minimum.

The transition state corresponding to ring fission on the $^3(\pi\pi^*)$ surface (Figure 3h) lies 17 kcal mol^{-1} above the $^3(\pi\pi^*)$ minimum (Figure 1i). This transition structure also leads to a twisted degenerate biradicaloid intermediate (Figure 3i), where the C−O π bond is fully formed and the unpaired electrons are on C_3 and C_2. This point corresponds to a $^3(\pi\pi^*)/S_0$ crossing point (Figure 3k), and intermediates on both $^3(\pi\pi^*)$ (Figure 3i) and S_0 (Figure 3j), although the minimum on S_0 could not be fully optimized as the surface is very flat in that region. The spin−orbit coupling computed at the $^3(\pi\pi^*)/S_0$ crossing point is <1 cm^{-1}, but the presence of the minimum on the triplet surface means that ISC to S_0 can occur after many molecular vibrations. The carbonyl bond can then rotate about the C_1-C_3 bond, with almost no barrier, to form the planar intermediate on S_0 (Figure 3g), located adjacent to the conical intersection which was mentioned above; the route to products is then the same as for the $^1(n\pi^*)$ state. An analogous planar intermediate (Figure 3l) also exists on the triplet surface and this has an energy lower than the intermediate on S_0.

Mechanism C: Oxadi-π-methane (ODPM)-Type Pathway. Mechanism C is initiated by the attack of the carbonyl carbon at C_2 (or C_1) to form a bicyclic biradical (Figure 4d−h) and the reaction path for acylcyclopropene could take place via an endo or an exo mechanism. A sketch of the endo pathway is shown in Figure 8. (The energies and structures for the exo pathway can be obtained as supporting information.) The "hub"

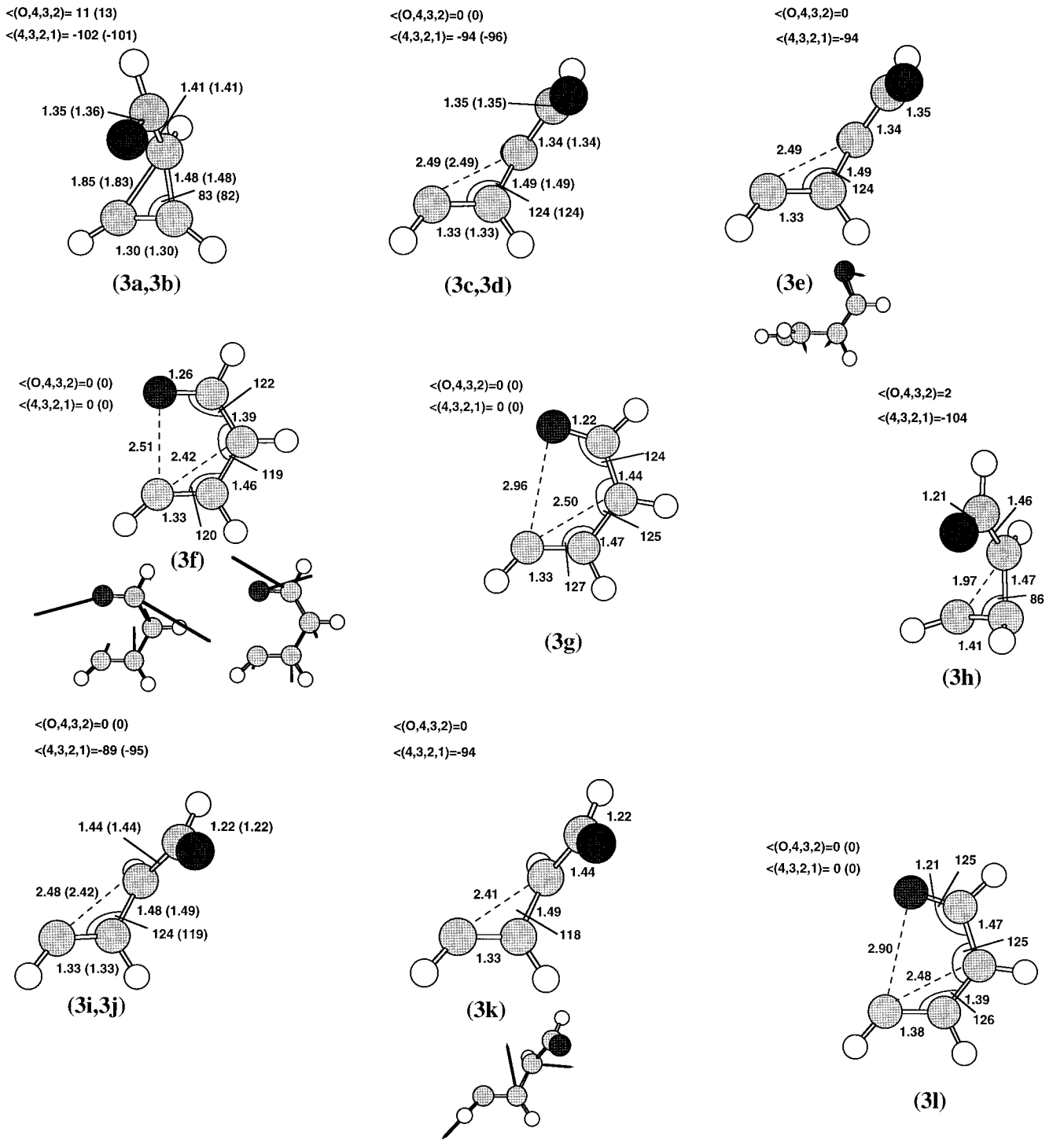

Figure 3. Optimized structures for initial ring-fission mechanism (bond lengths in angstroms and angles in degrees): (a) reactant minimum (syn)−twisted intermediate transition state on $^3(n\pi^*)$ surface; (b) reactant minimum (syn)−twisted intermediate transition state on $^1(n\pi^*)$ surface; (c) twisted intermediate on $^3(n\pi^*)$ surface; (d) twisted intermediate on $^1(n\pi^*)$ surface; (e) $^3(n\pi^*)/^1(n\pi^*)$ crossing point at twisted intermediate (with gradient difference vector shown below); (f) planar $^1(n\pi^*)/S_0$ conical intersection (with derivative coupling and gradient difference vectors shown below); (g) planar intermediate on S_0; (h) reactant minimum (syn conformation)−twisted intermediate transition state on $^3(\pi\pi^*)$ surface; (i) twisted intermediate on $^3(\pi\pi^*)$ surface; (j) twisted intermediate on S_0; (k) $^3(\pi\pi^*)/S_0$ crossing point at twisted intermediate (with gradient difference vector shown below); (l) planar intermediate on $^3(\pi\pi^*)$ surface. (At similar structures, singlet geometries are given in parentheses after the triplet geometries.)

of the mechanism is the 4-fold degenerate region of the bicyclic biradical where the $^1(n\pi^*)$, $^3(\pi\pi^*)$, $^3(n\pi^*)$, and ground state surfaces cross (analogous to the ODPM mechanism that occurs in acyclic β,γ-enones[15s] and efficient ISC and IC are both possible. The subsequent C_2-C_3 bond cleavage and C_2-O bond formation on S_0 is essentially a barrierless path to furan. Thus the process will be controlled by the barrier heights associated with C_2-C_4 bond formation to form the bicyclic biradical.

The endo reaction path from the syn conformer (Figure 1a) and the exo path from the anti conformer (Figure 1b) are very similar. At the decay regions for both endo and exo pathways we located conical intersections between S_1 and S_0 (Figure 4d) and between the two triplet surfaces (Figure 4e), at almost identical geometries. Furthermore, we have been able to characterize true minima corresponding to biradical intermediates on the $^3(\pi\pi^*)$, $^3(n\pi^*)$ and ground state surfaces (Figure 4f,g,h) near this point. The molecule in this region has a bicyclic

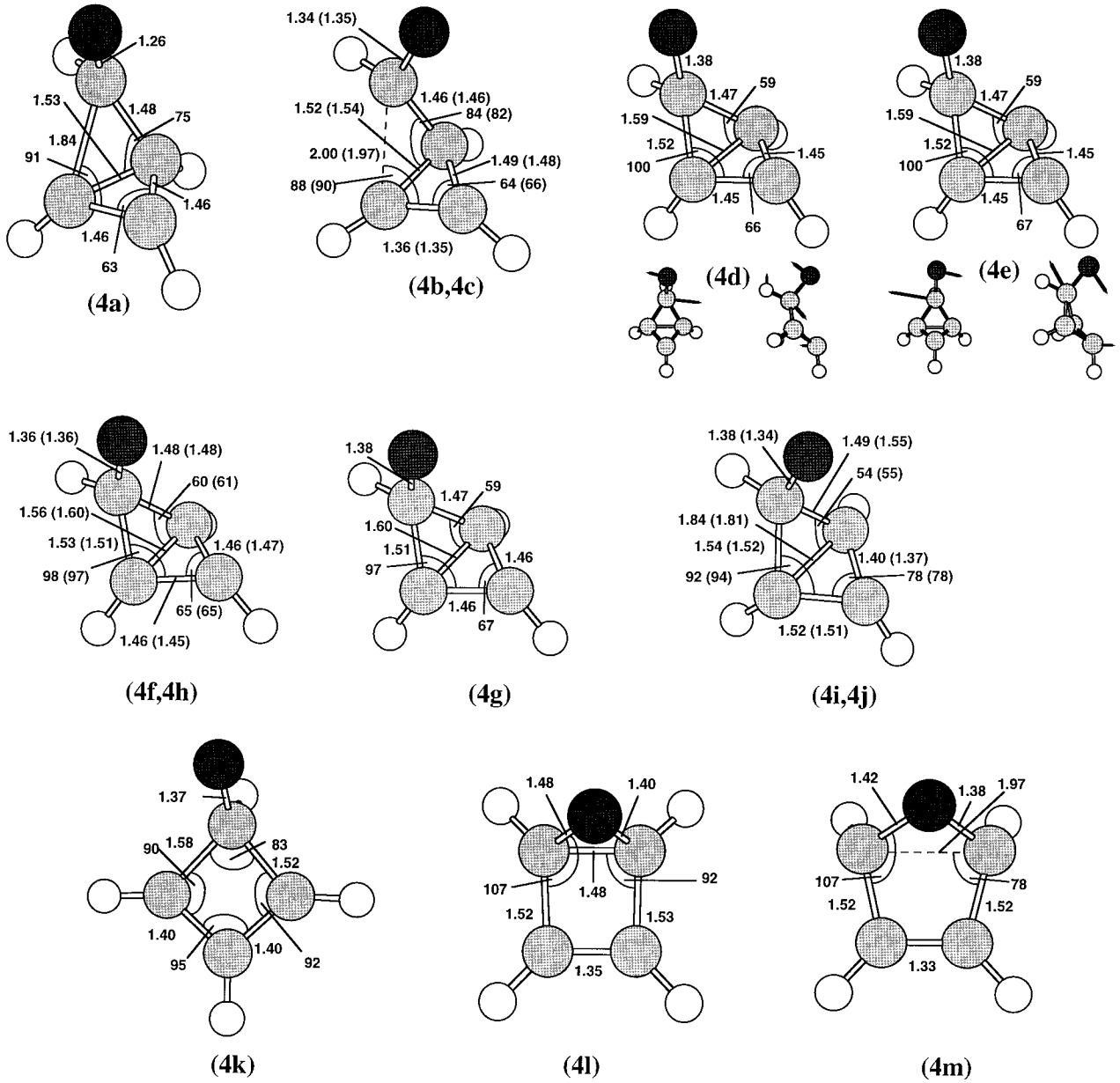

Figure 4. Optimized structures for ODPM-type mechanism−endo pathway (bond lengths in angstroms and angles in degrees): (a) reactant minimum (syn)−bicyclic intermediate transition state on $^3(\pi\pi^*)$ surface; (b) reactant minimum (syn)−bicyclic intermediate transition state on $^3(n\pi^*)$ surface; (c) reactant minimum (syn)−bicyclic intermediate transition state on $^1(n\pi^*)$ surface; (d) $^1(n\pi^*)/S_0$ conical intersection at bicyclic intermediate (with derivative coupling and gradient difference vectors shown below); (e) $^3(n\pi^*)/^3(\pi\pi^*)$ conical intersection at bicyclic intermediate (with derivative coupling and gradient difference vectors shown below); (f) Bicyclic intermediate on $^3(\pi\pi^*)$ surface; (g) bicyclic intermediate on $^3(n\pi^*)$ surface; (h) bicyclic intermediate on S_0; (i) bicyclic intermediate−square intermediate transition state on $^3(\pi\pi^*)$ surface; (j) bicyclic intermediate−square intermediate transition state on S_0; (k) square intermediate on $^3(\pi\pi^*)$ surface; (l) square intermediate on S_0; (m) square intermediate−furan transition state on S_0. (At similar structures, singlet geometries are given in parentheses after the triplet geometries.)

geometry with a new bond formed between C_2 and C_4. The unpaired electrons lie on the oxygen atom and C_1, but these two electrons are far enough apart that singlet and triplet states are degenerate. The singly and doubly occupied orbitals on the oxygen atom (an n orbital and a p orbital) are energetically equivalent, leading to two degenerate singlet or triplet states, giving rise to the four-level degeneracy. The value of the spin−orbit coupling is large (64−67 cm^{-1}) between triplet and singlet surfaces with different electronic configurations at the oxygen atom, but smaller ($\approx$1 cm^{-1}) between triplet and singlet surfaces with the same electronic configuration at the oxygen atom. However, the presence of the four-level degeneracy means that decay to the ground state will be efficient from all the excited state surfaces.

The transition states associated with C_2-C_4 bond formation from the excited state minima (Figure 1c−h) were located on

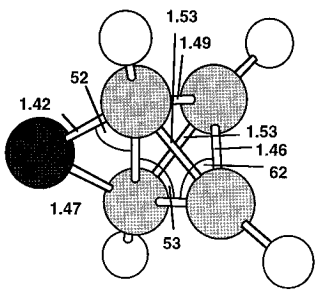

Figure 5. Optimized structure for mechanism via tricyclic intermediate (bond lengths in angstroms and angles in degrees): (a) tricyclic intermediate on S_0.

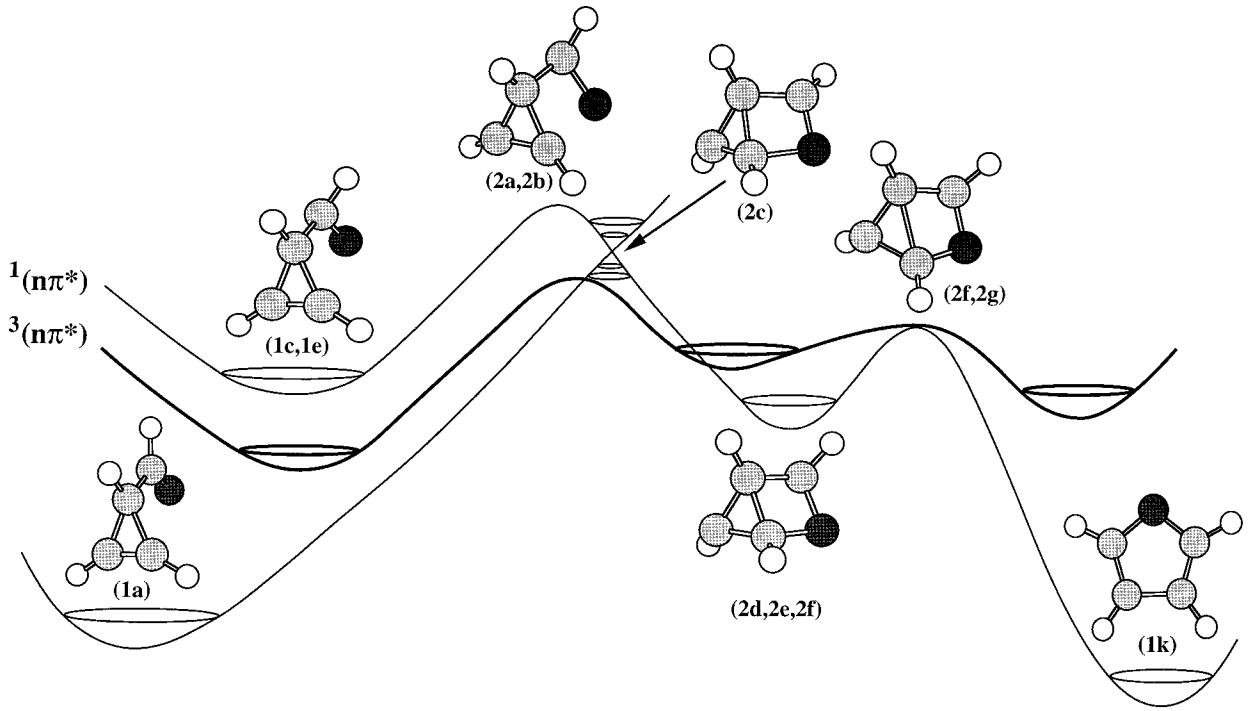

Figure 6. A schematic representation of the potential energy surface for the oxahousane mechanism.

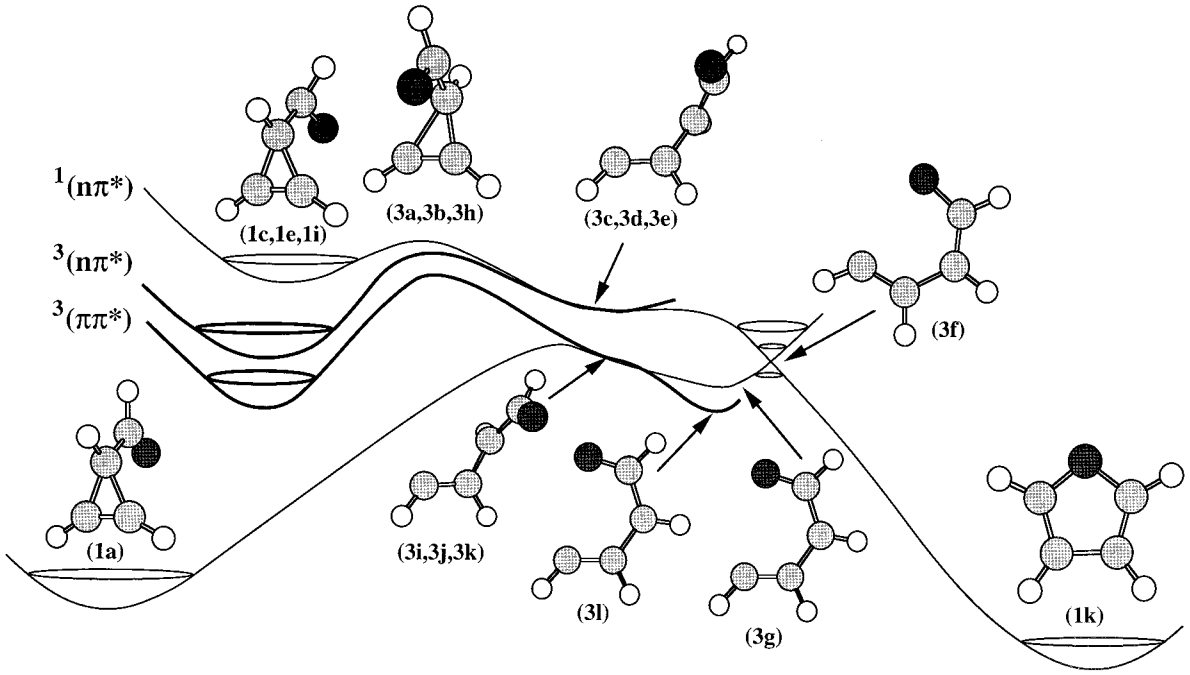

Figure 7. A schematic representation of the potential energy surface for the initial ring-fission mechanism.

all the excited state surfaces. The transition states on the $^3(n\pi^*)$ and $^1(n\pi^*)$ surfaces (Figure 4b,c) lie 4 and 1 kcal mol^{-1} respectively above the energy barriers leading to the oxahousane minimum, and some 24 kcal mol^{-1} above the barriers for initial ring fission. However, the transition state on the $^3(\pi\pi^*)$ surface (Figure 4c) lies some 20 kcal mol^{-1} below the $^3(n\pi^*)$ and $^1(n\pi^*)$ barriers and only 7 kcal mol^{-1} above the barrier to ring fission, indicating that this reaction would predominate from the $^3(\pi\pi^*)$ surface.

The degeneracy of the $^3(\pi\pi^*)$ state and S_0 persists along the reaction coordinate after the bicyclic biradical region, and transition states on both surfaces (Figure 4i,j) were located leading to a second biradical intermediate (Figure 4k) which has a four-membered ring of carbon atoms. The barriers on both the triplet and the ground state surface have almost the same energy. This second intermediate is well-defined on the triplet surface but is a very shallow minimum (or a shoulder) on the ground state surface and therefore no critical point could be optimized on this surface. However we were able to locate another shallow minimum on S_0, which occurs at a structure where the oxygen atom is bonded to C_3 (Figure 4l), and another transition state corresponding to C_4-C_3 bond cleavage (Figure 4m) leading from this minimum to furan.

Mechanism D: Synchronous Paterno-Buchi-Type Reaction. Mechanism D corresponds to a synchronous C=O + C=C Paterno−Buchi type mechanism via a tricyclic intermediate. We were unable to locate a structure of this type on the excited state surfaces, but it was located as a minimum on the ground state surface (Figure 5a). This point must be viewed as an intermediate between the four different oxahousane

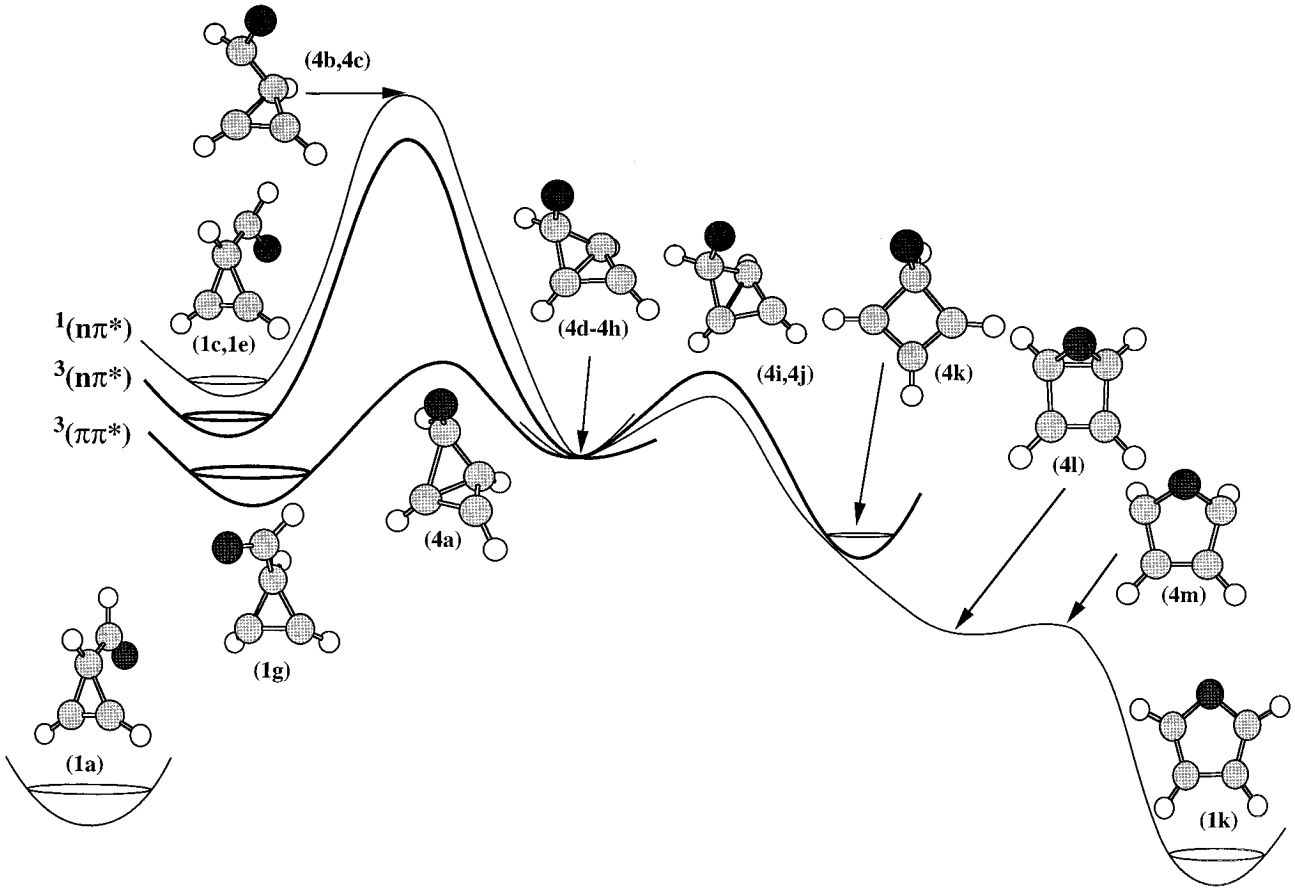

Figure 8. A schematic representation of the potential energy surface for the ODPM-type mchanism (endo pathway).

isomers. Cleavage of the C_2-C_3 bond first would lead to one isomer, whereas cleavage of the C_2-C_4 bond, the C_1-C_4 bond, or the C_1-C_3 bond would lead to other isomers. Any of these can then go on to form furan.

We were not able to locate a transition state between the tricyclic intermediate and the oxahousane minimum because the S_0 surface is very flat in this region. However, an IRC run *in the reverse direction* from the transition state (Figure 2h), which connects the oxahousane structure (Figure 2f) and furan (Figure 1i), simply passed straight through the shallow oxahousane intermediate and terminated a geometry close to this tricyclic intermediate. Therefore, for our model system, the tricyclic intermediate lies some 23 kcal mol^{-1} below the oxahousane intermediate and Mechanism D merges with Mechanism A. However, in the experiments of Zimmerman et al.,[1,2] the phenyl substitution will stabilize the biradicaloid structures relative to this tricyclic intermediate.

Conclusions

In this paper we have established the topology of the potential energy surfaces along four possible reaction coordinates (A−D) on the $^1(n\pi^*)$, $^3(n\pi^*)$, and $^3(\pi\pi^*)$ excited state surfaces of a "model" acylcyclopropene, that is without the phenyl substituents that were present in the mechanistic study of Zimmerman. In Mechanisms A, B, and C the initial step in the reaction takes place on the excited state surface, followed by efficient decay to the ground state surface via crossings that occur in the region of biradical intermediates. In all cases the remainder of the reaction coordinate lies on the ground state surface and is essentially barrierless. We have shown that all of the intermediates proposed by Zimmerman et al. exist; the most surprising result is their dual function as both minima and reaction funnels. However, for complex organic photochemical reactions of the type considered in this paper, the excited state energy barriers must play a major role. Here substituent effects will be very important and, in particular, the role of the phenyl group at biradical centers will stabilize the biradicaloid transition states in substituted acylcyclopropenes so that our energy barriers cannot be related directly to experiment. However, the existence of the crossing points is a fundamental feature of the electronic structures of the intermediates, and will not be affected by substituent effects.

Mechanisms A and B differ in the chronological sequence of the bond-breaking and bond-making processes. Zimmerman suggests that Mechanism A is favored for the triplet-substituted acylcyclopropenes while Mechanism B is operational for the singlet. Our results clearly establish that Mechanism A can only occur from the $n\pi^*$ surfaces, whereas a reaction path corresponding to Mechanism B exists on each of the $^1(n\pi^*)$, $^3(n\pi^*)$, and $^3(\pi\pi^*)$ surfaces. Our computed barriers imply that Mechanism B is the most favored pathway from all the excited states, in contrast to the experimental results of Zimmerman which indicate that although Mechanism B occurs on direct photolysis, Mechanism A occurs on triplet sensitization. Zimmerman et al. rule out Mechanism B for the triplet reaction on the grounds that they do not see the side products that are observed in the singlet reaction and ring-cleavage in cyclopropenes has been shown to be very unfavorable.[11] However, as the regioselectivity that would be observed in both reactions would be the same, they do not rule out the possibility that the actual mechanism that occurs could be a composit of both Mechanisms A and B.

The side products produced during the singlet reaction show that Mechanism B is almost certainly the reaction pathway that occurs on direct photolysis. Our results show that Mechanism B is the most favored reaction path from the $^1(n\pi)^*$ surface, in

agreement with the accepted mechanism. However, we found the intermediate in Mechanism B to be a biradical with the C_1-C_2 π bond still formed (C−C distance is 1.33 Å and therefore one of the electrons on C_2 remains fully paired with the electron on C_1), rather than a carbene-like structure (where one would have two unpaired electrons on C_2) as predicted by Zimmerman for the case of aryl-substituted vinylcyclopropenes.

Mechanism C (via the $^3(\pi\pi^*)$ state) is the pathway in triplet vinylcyclopropenes. Our results suggest that this pathway is also possible on the $^1(n\pi^*)$, $^3(n\pi^*)$, and $^3(\pi\pi^*)$ surfaces for our model acylcyclopropene compound but the barriers on the $n\pi^*$ surfaces are considerably higher than the barrier on the $\pi\pi^*$ surface such that the reaction would be unlikely to occur from the $n\pi^*$ surfaces. Therefore the reason why Mechanism C is not operative for triplet acylcyclopropenes is most probably because the $n\pi^*$ triplet state is populated preferentially to the triplet $\pi\pi^*$ state for Zimmerman's substituted molecules and this is why the reactions of acylcyclopropenes are different from those of both vinylcyclopropenes and β,γ-enones.

Acknowledgment. This research has been supported in part by the EPSRC and SERC (UK) under Grant Nos. GR/J25123 and GR/H58070. Sarah Wilsey is grateful to the EPSRC for a studentship.

Supporting Information Available: Mechanism C (exo pathway) and figures giving the optimized structure for the ODPM-type mechanism and a schematic representation of the potential energy surface for the ODPM-type mechanism (5 pages). This material is contained in many libraries on microfiche, immediately follows this article in the microfilm version of the journal, can be ordered from the ACS, and can be downloaded from the Internet; see any current masthead page for ordering information and Internet access instructions.

JA953726H